JOURNAL OF TAIBAH UNIVERSITY FOR SCIENCE
2024, VOL. 18, NO. 1, 2347057
https://doi.org/10.1080/16583655.2024.2347057

Mixed convection of ferrohydrodynamics magnetized hybrid ferrofluid on a slip-permeable stretching sheet

Nur Ilyana Kamis, Lim Yeou Jiann, Noraihan Afiqah Rawi and Sharidan Shafie

Department of Mathematical Sciences, Faculty of Science, Universiti Teknologi Malaysia, Johor, Malaysia

ABSTRACT

Mixed convection significantly affects fluid flow and heat transfer in manufacturing and engineering. This study investigates it in a ferrohydrodynamics magnetized hybrid ferrofluid on a slip stretching sheet affected by suction and injection. Using the modified Tiwari and Das model, the behavior of the hybrid ferrofluid, magnetite ferrite (Fe_3O_4) and cobalt ferrite ($CoFe_2O_4$) based-water and ethylene glycol are explored. The governing partial differential equations are simplified via a similarity technique and solved using the Keller box method. Forced convection reduces velocity profile and shear stress more rapidly than mixed and natural convection, exhibiting distinct thermal field and Nusselt number patterns. Injection increases shear stress by 71.98%, 83%, and 87.08% under forced, mixed, and natural convection, while suction raises it by 25.96%, 28.50%, and 28.53%, respectively. Under suction, natural convection drop by 5.12% Nusselt number, slightly less than forced (5.36%) and mixed convection (5.15%). Ferrohydrodynamics significantly influences flow and heat transfer.

ARTICLE HISTORY
Received 26 February 2024
Revised 18 April 2024
Accepted 19 April 2024

KEYWORDS
Mixed convection; suction and injection; ferrohydrodynamics; magnetized hybrid ferrofluid; slip stretching sheet

Nomenclature

U_w	stretching velocity
T_w	sheet temperature
T_∞	ambient or bulk temperature
T_c	Curie temperature
(u, v)	velocity components for (x, y)
ρ	density
μ	dynamic viscosity
ρC_p	heat capacity
k	thermal conductivity
T	temperature
M	magnetization
H	magnetic field
g	gravitational acceleration
β^*	thermal expansion
d	distance of the magnetic dipole
K	thermomagnetic
Pr	Prandtl number
ε	Curie temperature
χ	Viscous dissipation
δ	Partial slip
S	Suction and injection
β	Ferrohydrodynamic interaction parameter
α	Dimensionless distance
λ	Mixed convection
Gr_x	Grashof number
Re_x	Reynold number
C_f	Local skin friction
Nu_x	Nusselt number
τ_w	Wall shear stress
q_w	Heat transfer rate

1. Introduction

The processes of cooling and heating are fundamental thermodynamic operations that entail the transfer of heat within a fluid either to or from a system to achieve the desired temperature change. Heat transfer defined as the exchange of thermal energy between objects or regions due to temperature differences, plays a crucial role in these operations. In the realm of heat transfer, convection takes precedence over radiation and conduction in certain daily life scenarios due to its direct interaction with fluids – liquids or gases – that are prevalent in our environment. Conduction proves more effective in solid materials, while radiation can operate in a vacuum, making it less relevant in direct contact with fluids [1]. Within the context of convection, the significance of mixed convection becomes apparent when examining the concurrent influence of both fluid motion and external forces on heat transfer. Natural convection is driven by buoyancy forces resulting from temperature differences, and forced convection is induced by external means such as fans or pumps [2].

CONTACT Noraihan Afiqah Rawi noraihanafiqah@utm.my Department of Mathematical Sciences, Faculty of Science, Universiti Teknologi Malaysia, 81310 Johor Bahru, Johor, Malaysia

Understanding mixed convection in fluid flow is essential for optimizing heat transfer systems. The increase in buoyancy force corresponds to the enhancement of the mixed convection parameter, causing a significant reduction in the thermal boundary layer thickness as the fluid temperature decreases sharply along an inclined stretching sheet [3]. Mahdy [4] asserted that the mixed convection parameter improves heat transfer performance, as evidenced by the Nusselt number of fluid flows over a stretching surface. In addition, an incrementation is also observed in the velocity profile [5]. Daniel et al. [6] reported that the absence of the mixed convection parameter, assigned as forced convection flow, minimally affects fluid flow velocity. Conversely, the inclusion of the mixed convection parameter during natural convection leads to an increase in the velocity profile [6]. The shear stress development is higher in mixed convection, followed by natural convection and forced convection, as reported by Ishak et al. [7].

Permeable surfaces are commonly employed in heating and cooling systems. Typically, a permeable surface is associated with a scenario where the surface allows fluid to either be removed (suction) or introduced (injection or blowing) through its pores or openings [8]. The investigation of fluid flow with suction and injection effects was pioneered by Gupta and Gupta [9], who extended the work from Crane [10] beyond a stretching sheet. According to the analytical solution, an increase in suction causes a progressive thinning of the boundary layer, while the reverse is true for blowing. This is because suction entrains fluid from the ambient environment while blowing pushes fluid away from the surface [9]. Hence, suction and injection effects provide means to control and manipulate fluid flow. Subsequently, many researchers have focused on investigating fluid flow embedded within suction and injection effects. It is reported that transitioning from injection to suction retards the temperature profile [11]. This implies that an increase in the suction parameter leads to an elevation in the thermal boundary layer thickness [12]. With an increase in injection intensity, the fluid velocity is enhanced, while the suction effect improves the shear stress of the fluid [13]. Sandeep and Sulochana [14] argued that the presence of suction and injection parameters along a stretching sheet intensifies the heat transfer rate in fluid flow. However, Obalalu et al. [15] found that suction-based convective cooling proves more effective in influencing the thermal properties of the fluid compared to injection-based convective cooling. The valuable articles discussing suction and injection effects can be found in [16–22].

Besides, the slip effect – specifically slip boundary conditions – also plays a substantial role in impacting the heat transfer flow across various fluid dynamics scenarios. Slip conditions denote the relative motion between a fluid and a solid surface [23]. Velocity slip occurs when the fluid near a solid boundary has a velocity different from the solid surface [23]. In 1823, Navier took the initiative to incorporate slip boundary conditions into the examination of linear viscous fluid dynamics [24]. This initiative involved postulating a direct connection between the extent of relative slip length and the local shear stress. Following this, Andersson [25] conducted an initial analytical exploration into the influence of velocity slip on the flow around a stretching surface. As the slip factor increases, there is a corresponding elevation in slip magnitude, resulting in a decrease in frictional resistance between the viscous fluid and the surface. Building upon the work of [25], Wang [26] asserted that the outcomes from the analytical solution of Navier-Stokes with a slip stretching sheet can be extrapolated to applications in convective heat transfer and convective mass diffusion. These applications are particularly significant in processes like extrusion.

Thompson and Troian [27] proposed that the slip length of velocity remains constant, unaffected by temperature variations in fluid flow. Yazid et al. [28] discovered that the slip coefficient at the boundary conditions eliminates the local skin friction along the stretching sheet. Rajesh et al. [29] investigated the existence of partial slip at the fluid-solid interface, resulting in a diminished velocity distribution compared to a no-slip condition. This occurs because, in the absence of slip, the fluid velocity aligns with the velocity of the stretching sheet. An analytical solution presented by Turkyilmazoglu [30] illustrates that the partial slip parameter enhances convective heat transfer over conductive heat transfer in magnetohydrodynamic (MHD) fluid flow. The momentum boundary layer is reduced when considering velocity slip, however, the thermal boundary layer is thicker [31].

The impacts of velocity slip, as well as suction and injection effects, become particularly pronounced when the presence of nanoparticles in the fluid is taken into account. This is because the introduction of nanoparticles into the liquid creates conditions that deviate from the assumption of a perfectly smooth surface during fluid flow [16]. Moreover, the inclusion of nanoparticles leads to the formation of surface roughness or texture on a plate, inducing slippage and altering the initial velocity of the fluid [32]. Suction usually entails the removal of reactants or waste nanoparticles, whereas injection introduces new particles or reactants into the system [8]. This process enhances the stability of the heat transfer system, particularly with the presence of nanoparticles in fluid. It is crucial to note that incorporating nanoparticles in a fluid introduces the term nanofluid (NF). The concept of NF was introduced by Choi and Eastman in 1995 [33]. NF can indeed be prepared using physical or chemical methods, which involve dispersing nanoparticles in a base fluid [34]. It is noteworthy that nanoparticles in NF typically fall

within the 1 to 100 nanometer (nm) size range, a significant departure from the micrometer-sized particles described in Maxwell's concept [35]. The application of NF for industrial cooling has demonstrated positive outcomes, leading to energy conservation and a decrease in emissions [5].

Although the presence of nanoparticles in NF can enhance thermal conductivity, achieving both improved conductivity and stability in single-component NF poses a challenge. Stability concerns, such as particle agglomeration or sedimentation over time, may offset the benefits of increased conductivity, restricting their long-term practicality [36]. To address this trade-off, researchers have introduced hybrid nanofluids (HNF), which involve blending metallic and non-metallic nanoparticles to optimize both thermal properties and stability [37]. Investigations on HNF encompass metallic, non-metallic, and carbon materials [38]. Some researchers have directed their attention to HNF involving the inclusion of magnetic nanoparticles, specifically focusing on ferrite nanoparticles [39]. This type of HNF is commonly referred to as hybrid ferrofluid (HFF). It is important to point out that the thermal conductivity of HFF is higher than that of the normal base fluid, making them potentially superior candidates in heat transfer systems [40,41]. According to Raj and Boulton [42], the effective thermal conductivity of HFF relies on imposed magnetic field strength.

Magnetic field can be used to manage the heat transfer in a convective system, resulting in improved heat transfer characteristics [43]. Magnetic fields offer substantial potential across diverse applications, including the field of medical science [44]. Notably, a magnetic field presents a promising avenue for developing an alternative and potentially more effective drug delivery with fewer side effects compared to existing options. The interaction of magnetic fields with a fluid containing suspended magnetic nanoparticles gives rise to the intriguing phenomenon known as "ferrohydrodynamics" (FHD) and force known as the Kelvin force, resulting from fluctuations in field strength [45,46]. This process entails the manipulation and control of fluid motion induced by the interplay between magnetic nanoparticles and an external magnetic field [45].

Understanding the FHD is critical for inducing fluid movement. Therefore, HFF holds promising applications in various technical, industrial, and scientific fields. This is especially notable in the realm of biomedical engineering and technological fields, where they hold significant potential applications in biomedical applications (magneto-thermal therapy, targeted drug delivery, magnetic hyperthermia) [47–49], coating process [50], and magnetic cooling [51]. Neuringer and Rosensweig [52] provided an analytical solution, revealing that the thermal energy of the fluid increases when subjected to the FHD effect. Based on the theoretical study reported by Rosensweig [45], as the magnetic dipole-induced magnetic field intensity rises, the fluid reaches saturation. Consequently, the FHD effect leads to a decrease in the heat transfer rate, and it simultaneously causes an increase in shear stress [53,54]. A magnetic dipole is one type of source that generates magnetic fields. It is a magnet or magnetic material where one end has a north pole, and the other end has a south pole [55]. A condensed magnetic spherical bar yields more robust magnetic fields owing to its closely spaced dipoles, thereby generating a uniform and intensified magnetic field in its vicinity. On the other hand, an applied magnetic field can be either external or induced within the fluid, as seen in phenomena like magnetohydrodynamics (MHD). This magnetic field interacts with the moving charged particles, such as ions and electrons, within the fluid. This interaction leads to the induction of a Lorentz force, which plays a pivotal role in driving the dynamics and behavior of the fluid [56].

It is worth noting that the researchers employed ferrite nanoparticles comprised of iron-oxide compounds such as magnetite ferrite (Fe_3O_4), nickel zinc ferrite ($NiZnFe_2O_4$), manganese zinc ferrite ($MnZnFe_2O_4$) and cobalt ferrite ($CoFe_2O_4$) to examine the behavior of the boundary layer flow. Notably, Fe_3O_4 exhibits higher magnetic strength and thermal conductivity in comparison to $NiZnFe_2O_4$ and $MnZnFe_2O_4$ attributed to its lower velocity profile and higher temperature field [57]. Similarly, $CoFe_2O_4$ demonstrates superior saturation magnetization and heat transfer capability compared to other ferrite nanoparticles like Fe_3O_4, $NiZnFe_2O_4$, and $MnZnFe_2O_4$, even in the absence of an external magnetic field [58,59]. It is intriguing to highlight that $CoFe_2O_4$ displays ferromagnetic behavior and exceptional chemical stability, positioning it as a robust magnetic material with potential applications in medical fields, such as hyperthermia cancer therapy [60]. Therefore, the theoretical studies reported by Anantha Kumar et al. [61] claimed that the heat transfer of $Fe_3O_4/CoFe_2O_4$ improves HFF flow compared to ferrofluid flow. The examination of hybrid ferrofluid (HFF) in the literature is detailed in Table 1, encompassing the impacts of mixed convection (MC), ferrohydrodynamics (FHD), suction and injection effects (SIE), and velocity slip (VS).

Table 1. Previous studies on HFF.

Authors	HFF	MC	FHD	SIE	VS
[62]	Fe_3O_4 and molybdenum disulfide (MoS_2)	√	×	×	×
[63,64]	$NiZnFe_2O_4$ and $MnZnFe_2O_4$	×	√	×	×
[65]	Fe_3O_4 and $MnZnFe_2O_4$	×	√	×	×
[66]	Fe_3O_4 and $CoFe_3O_4$	√	×	√	×
[67]	$CoFe_2O_4$ and $MnZnFe_2O_4$	×	×	√	×
[68]	$NiZnFe_2O_4$ and $MnZnFe_2O_4$	×	×	×	√
[69,70]	Fe_3O_4 and copper (Cu)	×	×	√	√
[71]	Fe_3O_4 and $CoFe_3O_4$	√	×	×	×
[72]	$CoFe_3O_4$ and copper oxide (CuO)	×	√	×	×

Based on the information presented in Table 1, it is evident that no prior studies have explored the mixed convection of a hybrid ferrofluid (HFF) composed of Fe_3O_4 and $CoFe_3O_4$ in the presence of a magnetic dipole, suction and injection effects, and velocity slip. Therefore, this study aims to address this research gap with the following objectives:

i. to explore the effect of the magnetic dipole and the induced ferrohydrodynamics (FHD) interaction in HFF flow,
ii. to investigate and compare free convection, forced convection, and mixed convection concerning the examined parameters in HFF flow.
iii. to explore and discuss the partial slip and suction/injection effects on FHD HFF flow.

To accomplish these objectives, the governing equations are developed based on previous studies [7,12, 28,65] in the form of partial differential equations (PDEs). These complex PDEs are then transformed into a set of coupled dimensionless ordinary differential equations (ODEs) using appropriate dimensionless variables. The resulting ODEs are solved using an implicit finite-difference method known as the Keller box method, as described in the book by Cebeci and Bradshaw [73]. The outcomes, including profiles and physical quantities for the investigating parameters, are presented, analyzed, and visualized through graphs and tables.

2. Mathematical formulation

2.1. Ferrohydrodynamics (FHD) effect

Ferrohydrodynamics (FHD) involves the study of the interaction between magnetic fields and fluid flow containing suspended magnetic particles, typically at the nanoscale. It explores the influence of magnetic forces on the behavior of hybrid ferrofluids (HFF) that contain ferromagnetic particles [45]. In this context, the magnetic dipole serves as the source of magnetic fields and is positioned below the $x-$axis at a distance, d (see Figure 1). The center of the magnetic dipole aligns with the $y-$axis, as depicted in Figure 1 [65]. The magnetic fields generated are perpendicular to the $x-$axis and saturate the HFF. The magnetic scalar potential, ω is defined as [65]

$$\omega = \frac{\gamma_1}{2\pi}\frac{x}{x^2+(y+d)^2}, \tag{1}$$

γ_1 is the source of the magnetic field strength (H). The two-dimensional representation of H can be expressed as $H = (H_x, H_y)$ [65]

$$\frac{\partial H}{\partial x} = -\frac{\partial \omega}{\partial x} = \frac{\gamma_1}{2\pi}\frac{x^2-(y+d)^2}{\left(x^2+(y+d)^2\right)^2}, \tag{2}$$

$$\frac{\partial H}{\partial y} = -\frac{\partial \omega}{\partial y} = \frac{\gamma_1}{2\pi}\frac{2x(y+d)}{\left(x^2+(y+d)^2\right)^2}. \tag{3}$$

As the magnetic body force is directly related to the gradient of H, the resultant magnitude of H is expressed as [65]

$$H = \left[\left(\frac{\partial \omega}{\partial x}\right)^2 + \left(\frac{\partial \omega}{\partial y}\right)^2\right]^{\frac{1}{2}}. \tag{4}$$

Expanding equations (2) and (3) based on equation (4) yields the following expressions [65]

$$\frac{\partial H}{\partial x} = -\frac{\gamma_1}{2\pi}\frac{2x}{(y+d)^4}, \tag{5}$$

$$\frac{\partial H}{\partial y} = \frac{\gamma_1}{2\pi}\left(-\frac{2}{(y+d)^3} + \frac{4x^2}{(y+d)^5}\right). \tag{6}$$

The change in magnetization (M) can be viewed as a linear relationship with temperature (T) [65]

$$M = K(T_c - T). \tag{7}$$

The thermomagnetic (K) effect induced by a thermal gradient on the magnetic properties of materials. Two conditions are necessary for the occurrence of the FHD effect [54,65]

i. the fluid must have T distinct from the Curie temperature (T_c) and
ii. an inhomogeneous magnetic field must be applied.

In fluid containing suspended magnetic nanoparticles, the magnetization of the magnetic material decreases when it reaches T_c. This characteristic is particularly significant in practical applications due to the notably high T_c of iron, approximately 1043 K [31].

2.2. Hybrid ferrofluid (HFF)

The experimental studies by Shoghl et al. [74], Colak et al. [75] and Colak [76] consistently support the theoretical model put forth by Tiwari and Das [77]. Consequently, this study employs a modified version of Tiwari and Das's model [77] to characterize the thermophysical properties of the hybrid ferrofluid (HFF). The density (ρ_{hff}) and specific heat ($(\rho C_p)_{hff}$ are expressed as follows [65]

$$\rho_{hff} = (1-\phi_2)[(1-\phi_1)\rho_{bf} + \phi_1\rho_{s_1}] + \phi_2\rho_{s_2},$$

$$(\rho C_p)_{hff} = (1-\phi_2)[(1-\phi_1)(\rho C_p)_{bf} + \phi_1(\rho C_p)_{s_1}] + \phi_2(\rho C_p)_{s_2}.$$

Brinkman [78] introduced the dynamic viscosity (μ_{hff}) which represents the higher concentration of spherical nanoparticles is applied

$$\mu_{hff} = \frac{\mu_{bf}}{(1-\phi_1)^{2.5}(1-\phi_2)^{2.5}},$$

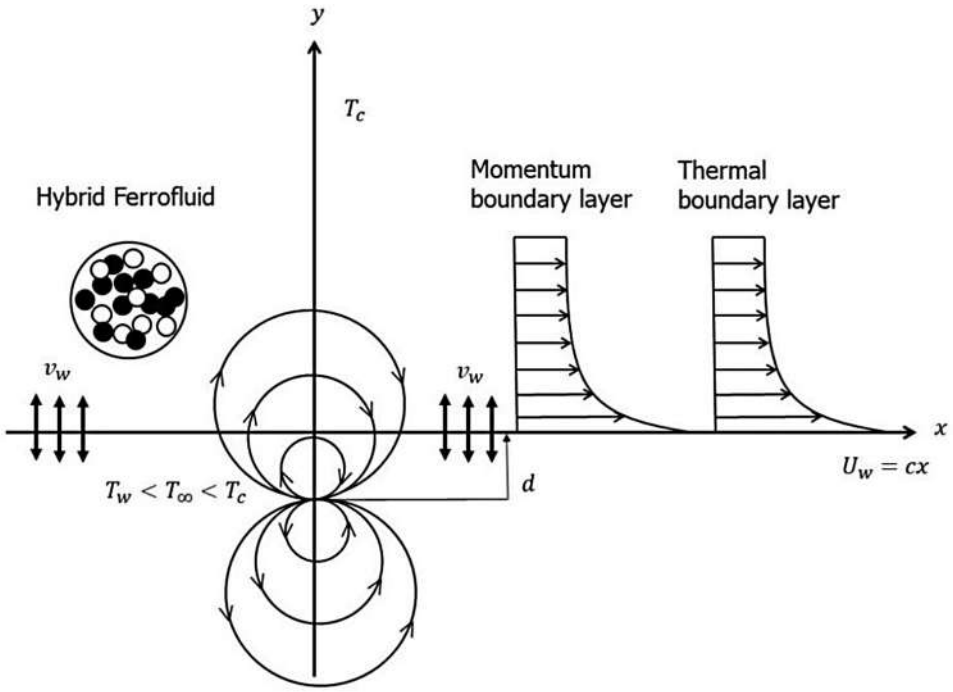

Figure 1. Physical geometry.

Table 2. The thermophysical traits of HFF [61,66].

Properties	$Fe_3O_4(\phi_1)$	$CoFe_2O_4(\phi_2)$	Ethylene glycol with water (50%-50%)
$\rho(kgm^{-3})$	5180$[\rho_{s_1}]$	4907$[\rho_{s_2}]$	1056$[\rho_{bf}]$
$C_p(Jkg^{-1}K^{-1})$	670 $[(C_p)_{s_1}]$	700$[(C_p)_{s_2}]$	3.288$[(C_p)_{bf}]$
$k(Wm^{-1}K^{-1})$	9.7$[k_{s_1}]$	3.7$[k_{s_2}]$	0.425$[k_{bf}]$
Pr	-	-	29.86

while the thermal conductivity (k_{hff}) approximated by Maxwell's model, is given [79]

$$k_{hff} = \frac{k_{s_2} + 2k_{ff} - 2\phi_2(k_{ff} - k_{s_2})}{k_{s_2} + 2k_{ff} + \phi_2(k_{ff} - k_{s_2})} \times k_{ff}$$

Where

$$\frac{k_{ff}}{k_{bf}} = \frac{k_{s_1} + 2k_{bf} - 2\phi_2(k_{bf} - k_{s_1})}{k_{s_1} + 2k_{bf} + \phi_2(k_{bf} - k_{s_1})},$$

The superscripts s_1, s_2, bf, ff, ϕ_1, and ϕ_2 denote the first and second solid nanoparticles, base fluid, ferrofluid, and first and second nanoparticle volume fractions, respectively. The thermophysical for HFF with conventional fluid are presented in Table 2.

2.3. The governing equations

Based on the assumptions, this study is dedicated to examine the characteristics of boundary layer flow and heat transfer in a specific hybrid ferrofluid (HFF). This particular HFF is composed of magnetite ferrite (Fe_3O_4) and cobalt ferrite ($CoFe_2O_4$). Both ferrite nanoparticles are dissolved in a conventional fluid, namely an ethylene glycol (EG) and water solution. The HFF is represented in a two-dimensional space with velocity components (u, v) at (x, y) directions. The fluid is considered incompressible and laminar, experiencing boundary layer flow over a stretched sheet. The analysis takes into account the influence of mixed convection involving the magnetic dipole and partial slip velocity as the fluid passes over a flat sheet. Suction and injection effects are considered in the study. The HFF induces its motion by stretching an elastic sheet along the $x-$axis, with the $y-$axis perpendicular to the sheet, as shown in Figure 1 [65]. The sheet undergoes stretching with a velocity $U_w = cx$, where $c > 0$ denotes the rate of stretching [65]. The sheet is maintained at a constant temperature (T_w), and the surrounding fluid is denoted as T_∞. The presence of magnetic nanoparticles in the fluid introduces a specific temperature known as the Curie temperature (T_c). When the fluid temperature surpasses T_c, the HFF undergoes a transition, losing its magnetism and transforming into a paramagnetic state. In this state, the temperature of the HFF system follows the condition $T_w < T_\infty < T_c$ [65]. Hence, the governing PDEs are established as follow [30,65]

$$\frac{\partial u}{\partial x} + \frac{\partial v}{\partial y} = 0, \tag{8}$$

$$\rho_{hff}\left(u\frac{\partial u}{\partial x} + v\frac{\partial u}{\partial y}\right) = M\mu_0\frac{\partial H}{\partial x} + \mu_{hff}\left(\frac{\partial^2 u}{\partial x^2} + \frac{\partial^2 u}{\partial y^2}\right) + g\beta^*(T_c - T), \tag{9}$$

$$(\rho C_p)_{hff}\left(u\frac{\partial T}{\partial x} + v\frac{\partial T}{\partial y}\right) + \left(u\frac{\partial H}{\partial x} + v\frac{\partial H}{\partial y}\right)\mu_0 T\frac{\partial M}{\partial T}$$

$$= k_{hff}\left(\frac{\partial^2 T}{\partial x^2}+\frac{\partial^2 T}{\partial y^2}\right) + \mu_{hff}\left[2\left(\frac{\partial u}{\partial x}\right)^2+2\left(\frac{\partial v}{\partial y}\right)^2+\left(\frac{\partial u}{\partial y}+\frac{\partial v}{\partial x}\right)^2\right]. \tag{10}$$

Here, equation (8) demonstrates the continuity equation. The final term in momentum equation (9) accounts for the mixed convection parameter, taking into consideration the gravitational field (g), and thermal expansion coefficient, (β^*) [66]. The term magnetic body force per unit volume of $M\mu_0\frac{\partial H}{\partial x}$ illustrates the components of magnetization force, commonly referred to as the Kelvin force [31,54]. This force diminishes when there is no magnetic gradient. In this context, μ_0 stands for the permeability of free space. In equation (10), the second term on the left-hand side signifies the heating due to adiabatic magnetization in HFF [31,54]. The concluding term in the energy equation (10) denotes viscous dissipation, serving as a heat source generated by fluid particle friction in HFF [31,54]. While magnetohydrodynamics (MHD) theory allows for a non-zero Lorentz force in the presence of a uniform magnetic field, FHD interactions necessitate a magnetic field that varies spatially, specifically distinguished by $\left(\frac{\partial H}{\partial x},\frac{\partial H}{\partial y}\right)$ [80]. Then, the boundary conditions are assumed as slip conditions together with suction and injection effect at the sheet $y=0$ [12,28,65]

$$y=0: u-U_w=L_{slip}\frac{\partial u}{\partial y}, v=v_w, T=T_w, \tag{11}$$

Here, the slip length (L_{slip}) and $\frac{\partial u}{\partial y}$ represents shear stress at the solid-fluid interface were defined with y denoting coordinates tangential to the surface. In addition, L_{slip} is assumed to be temperature-independent [27]. The suction and injection effects are defined as v_w and are established using the similarity transformation approach [12]. Meanwhile, the boundary conditions at a distance far from the sheet, where $y\to\infty$, are reformulated as [65]

$$y\to\infty: u=0, T=T_c. \tag{12}$$

2.4. Similarity transformations

The complexity of governing PDEs (8) to (10), along with their respective boundary conditions (11) and (12), have been reduced to ODEs by applying similarity transformations using the similarity variables as given below [65]

$$\psi(\eta,\xi)=\nu_f\xi f(\eta), \eta=\left(\frac{c\rho}{\mu}\right)^{\frac{1}{2}}y, \xi=\left(\frac{c\rho}{\mu}\right)^{\frac{1}{2}}x,$$
$$\theta(\eta,\xi)=\frac{T_c-T}{T_c-T_w}=\theta_1(\eta)+\xi^2\theta_2(\eta). \tag{13}$$

Here, $\nu_f=\frac{\mu}{\rho}$ demonstrates as kinematic viscosity. $\psi(\eta,\xi)$ represents the stream function, and $\theta(\eta,\xi)$ denotes the dimensionless temperature, both dependent on two independent variables (η,ξ). It is noteworthy that the equation for $\psi(\eta,\xi)$ satisfies the continuity equation (8), which is expressed as $u=\frac{\partial\psi}{\partial y}=cxf'(\eta)$ and $v=-\frac{\partial\psi}{\partial x}=-\left(\frac{c\mu}{\rho}\right)^{\frac{1}{2}}f(\eta)$. The velocity for suction and injection effects are given by $v_w=-\left(\frac{c\mu}{\rho}\right)^{\frac{1}{2}}f(0)$ [12]. Substituting equation (13) into governing PDEs (9) and (10) yields

$$\left(\frac{\mu_{hff}}{\mu_{bf}}\right)f'''-f'^2+ff''-\frac{2(\mu_{bf}/\mu_{hff})\beta\theta_1}{(\eta+\alpha)^4}+\left(\frac{\rho_{hff}}{\rho_{bf}}\right)\left(\frac{\mu_{hff}}{\mu_{bf}}\right)\lambda\theta_1=0, \tag{14}$$

$$\left(\frac{k_{hff}}{k_{bf}}\right)(\theta_1''+2\theta_2)+\left(\frac{(\rho C_p)_{hff}}{(\rho C_p)_{bf}}\right)Prf\theta_1'+\frac{2\chi\beta f(\theta_1-\varepsilon)}{(\eta+\alpha)^3}-\left(\frac{\mu_{hff}}{\mu_{bf}}\right)4\chi f'^2=0, \tag{15}$$

$$\left(\frac{k_{hff}}{k_{bf}}\right)\theta_2''-\left(\frac{(\rho C_p)_{hff}}{(\rho C_p)_{bf}}\right)Pr(2f'\theta_2-f\theta_2')+\frac{2\chi\beta f\theta_2}{(\eta+\alpha)^3}-\lambda\beta(\theta_1-\varepsilon)\left[\frac{2f'}{(\eta+\alpha)^4}+\frac{4f}{(\eta+\alpha)^5}\right]-\left(\frac{\mu_{hff}}{\mu_{bf}}\right)\chi f''^2=0. \tag{16}$$

The boundary conditions (11) and (12) become at

$$\eta=0: f(\eta)=S, f'(\eta)=1+\delta f''(\eta), \theta_1(\eta)=1, \theta_2(\eta)=0, \tag{17}$$

at

$$\eta\to\infty: f'(\eta)\to 0,\ \theta_1(\eta)\to 0,\ \theta_2(\eta)\to 0. \tag{18}$$

Where the prime symbol denotes the derivative with respect to η. S for suction ($S>0$) and injection ($S<0$). The dimensionless parameters are listed in Table 3.

2.5. Engineering parameters

Studying local skin friction, C_f and Nusselt number, Nu_x in engineering are crucial because they provide key insights into the behavior of fluid and heat transfer within a system. Understanding C_f helps engineers comprehend the resistance experienced by fluids as they flow past a surface. The parameter C_f in terms of wall shear stress, τ_w is defined as [54,65]

$$C_f=-\frac{2\tau_w}{\rho_{bf}U_w^2}, \text{where } \tau_w=\mu_{hff}\left.\frac{\partial u}{\partial y}\right|_{y=0}.$$

Meanwhile, the Nu_x provides information about heat transfer efficiency between a solid surface and a fluid, aiding in the design of cooling systems, heat

Table 3. Dimensionless parameter.

Symbol	Model parameter	Mathematical expression
Pr	Prandtl number	$\frac{\mu C_\rho}{k}$,
ε	Curie temperature	$\frac{T_c}{T_c - T_w}$,
χ	Viscous dissipation	$\frac{c\mu^2}{\rho k(T_c - T_w)}$,
β	FHD interaction	$\frac{\gamma}{2\pi}\frac{\mu_0 K(T_c - T_w)\rho}{\mu^2}$,
α	Dimensionless distance	$\sqrt{\frac{c\rho}{\mu}}d$,
λ	Mixed convection parameter	$\frac{Gr_x}{Re_x^2} = \frac{\left[\frac{g\beta^*(T_c-T)}{c^2 x}\right]}{Re_x^2} = \frac{g\beta^*(T_c - T)x^3}{{\nu_f}^2}$,
δ	First-order velocity slip	$L_{slip}\left(\frac{c\rho}{\mu}\right)^{\frac{1}{2}}$.

exchangers, and thermal management in various engineering applications. The parameter Nu_x with heat transfer rate q_w is written as [65]

$$Nu_x = \frac{xq_w}{k_{bf}(T_c - T_w)}, \text{where } q_w = -k_{hff}\frac{xq_w}{k_{bf}(T_c - T_w)}.$$

The dimensionless forms of C_f and Nu_x in relation to the Reynolds number, Re are derived through the application of similarity variables (14), resulting as [65]

$$C_f Re_x^{\frac{1}{2}} = -\frac{2}{\mu_{hff}} f''(0) \text{and } Nu_x Re_x^{-\frac{1}{2}} = -\frac{k_{hff}}{k_{bf}}[\theta_1'(0) + \xi^2\theta_2'(0)].$$

3. Numerical method

The resulting ODEs (14) to (18) are solved using the Keller box method, which is well-known for addressing nonlinear parabolic problems. This method is chosen due to its unconditional stability, enabling reliable computations [73]. It involves discretizing the domain into a grid and approximating the solution at each grid point. Not only is this numerical scheme more accessible, but it is also highly adaptable and practical compared to other methods. Consequently, the iterative process through this method yields highly accurate numerical outputs [81]. The primary steps to comprehend the workflow of this method are revealed below.

i. The resulting ODEs (14) to (18) reduce to first order system by introducing the new dependent variables of $f(\eta), u(\eta), v(\eta), \theta(\eta)$ and $g(\eta)$.
ii. The first-order derivative equations, as indicated in step (i), undergo the application of numerical techniques utilizing finite difference schemes. The central difference scheme is employed to discretize equations (14) to (16). This process results in the generation of nonlinear algebraic system equations. The boundary conditions (17) and (18) are also discretized at $x = x^i$.
iii. The iterations are introduced to linearize the nonlinear algebraic system in step (ii) through the Newton method.
iv. The linear algebraic system is converted into a matrix and solved using the block tri-diagonal factorization scheme. It is crucial to note that the block tri-diagonal matrix is distinctive due to its composition of matrix blocks. Subsequently, the Thomas algorithm of a block-elimination technique is applied to achieve the numerical solutions of the matrix.

The computational procedure of the Keller box method is implemented using MATLAB software, followed by the generation of corresponding numerical results. Comprehensive information regarding the Keller box method can be referenced in works [73,82,83].

4. Results and discussion

The present study delves into the impact of the magnetic dipole on the behavior of a hybrid ferrofluid (HFF) as it flows past a stretching porous sheet. Various factors are taken into consideration in the investigation, including ferrohydrodyhamics (FHD) interaction (β), suction and injection (S), partial velocity slip (δ), the volume fraction of magnetic nanoparticles (ϕ_2), and the mixed convection parameter (λ). The smart HFF is synthesized by blending magnetite ferrite (Fe_3O_4) and cobalt ferrite ($CoFe_2O_4$) into a biopolymer solution, which is a mixture of ethylene glycol (EG) and water. This HFF solution shows potential applications in heating and cooling systems [47,48,50,51]. To underscore the significance of the effects, the analysis is initiated by configuring the parameters without the investigated variable and subsequently adjusting the values based on previous research findings. The examination is conducted by categorizing it into three scenarios: forced convection,$\lambda = 0$, mixed convection, $\lambda = 1.0$ and natural convection, $\lambda = 1.2$ [7]. Additionally, suction ($S > 0$) and injection ($S < 0$) are also compared against the pertinent parameters [15]. The parameters for both the initial and investigated parameters are established as follows.

Initial parameters:

$$\text{Initial parameters : } Pr = 29.86[64],$$

$$\varepsilon = 2.0, \chi = 0.01 \text{and } \alpha = 1.0[57]$$

$$\text{Investigated parameters : } \delta = \{0.0, 0.3, 0.5\}[32],$$

$$\beta = \{0.0, 1.0, 2.0\}[60], \phi_2 = \{0.00, 0.01, 0.02\}[65]. \quad (20)$$

4.1. Verification of the results

Several parameters have been compared with those of the previous study, as outlined in Tables 4 and 5. Table 4 shows the code validation for the mixed convection parameter λ, while Table 5 presents the partial velocity slip parameter δ and suction parameter S examined in the current study. It is clear that the current study presents a comparable solution to the previous investigations [5,53], with the mixed convection parameter set to $\lambda = 1$ corresponding to local skin friction ($f''(0)$) in Table 4. When the current study converges to a limiting case by setting $\beta = \lambda = \phi_1 = \phi_2 = 0$ and taking $Pr = 7$, the numerical results for $f''(0)$ demonstrate good agreement with published studies [25,26] in the absence of the suction effect ($S = 0$), as depicted in Table 5. A comparable result is also evident in the case of the suction effect ($S = 2$) when comparing the current study with a prior investigation [30]. It is notable that $f''(0)$ decreases as the parameter δ raises. Remarkably, an elevated value of $f''(0)$ is observed in the presence of the suction effect, $S = 2$ than $S = 0$ along a slip stretching sheet, particularly when δ is set to 1.0 and 5.0. Therefore, the findings of this current study align well with the existing results, providing confidence in the computation and analysis of the remaining tasks within the study.

4.2. Ferrohydrodyhamics (FHD) Interaction (β)

The reaction between a fluid containing suspended ferrite nanoparticles and magnetic fields leads to the FHD effect. This phenomenon is observed by considering the dimensionless FHD interaction parameter (β), the dimensionless distance of the magnetic dipole from the origin (α), and the Curie temperature (ε). Figure 2(a) is plotted to illustrate the velocity profile ($f'(\eta)$) due to the parameter β. It is noteworthy that $f'(\eta)$ decreases as the parameter β increases from 0 to 2 past a stretching sheet. When ferrite nanoparticles respond to magnetic fields, they tend to align themselves along the direction of the fields, forming structures often referred to as magnetic chains or clusters, saturating the HFF. As these magnetic chains develop, they have a noticeable impact on the rheological properties of the HFF, typically resulting in an increase in viscosity. The heightened viscosities limit the movement of the fluid, creating increased resistance to its flow. This finding aligns with the conclusions presented by Andersson [54].

Figure 2(a) also depicts the influence of the mixed convection parameter (λ) on the flow of HFF, magnifying the parameter β. It is evident that $f'(\eta)$ drastically declines in forced convection as $\lambda = 0$ compared to $\lambda = 1$ for mixed convection and $\lambda = 1.2$ for natural convection. This phenomenon arises due to the presence of buoyancy forces as the dimensionless parameter λ transitions from 0 to 1.2. Referring to Table 3, λ is defined as the ratio of the Grashof number (Gr_x) to the Reynolds number (Re_x). Gr_x is directly associated with buoyancy force and inversely related to viscous force. Therefore, the lack of buoyancy force in HFF flow reduces the momentum boundary layer. It is also observed that the removal of the reactants through the intensity of suction ($S > 0$) obviously lowers $f'(\eta)$ compared to the injection process ($S < 0$). This means that removing the HFF has diminished the pressure in the HFF system, thereby reducing the force between the nanoparticles when stretching the elastic sheet.

Besides influencing the velocity field, the parameter β significantly affects the temperature profile ($\theta_1(\eta)$), as demonstrated in Figure 2(b). The presence of the parameter β generating the FHD effect enhances heat content in the HFF. As β increases, a stronger alignment of ferrite nanoparticles occurs in response to the magnetic fields, leading to heat generation through the realignment of magnetic moments. Simultaneously, this alignment enhances convective heat transfer within the HFF, creating more effective pathways for heat transfer from the solid surface. Hence, the temperature field elevates, accompanied by an accumulation in the thermal boundary layer. Notably, it is also observed in Figure 2(b) that $\theta_1(\eta)$ is detected lower in the case of $\lambda = 1.2$ than in cases with $\lambda = 1$ and $\lambda = 0$. This implies that a greater buoyancy force, at its maximum with $\lambda = 1.2$, impedes the accumulation of heat in the HFF system. Hence, natural convection results in a thinner thermal boundary layer within the HFF system rather than forced and mixed convection. Simultaneously, the injection process, which introduces reactant into the HFF system, results in the accumulation of more heat in the fluid. Therefore, $\theta_1(\eta)$ with the injection case is higher than $\theta_1(\eta)$ with the suction case.

4.3. Partial Velocity Slip (δ)

Figure 3(a) has been generated for the purpose of analyzing the effects of the partial slip parameter, δ on $f'(\eta)$. The result illustrates that as the parameter δ increases along a stretching sheet, the motion of the HFF progressively decreases. This pattern occurs due to the heightened influence of lubrication and surface slippage, which hinders the free movement of nanoparticles. Consequently, the momentum boundary layer becomes thinner and approaches closer to the surface of the sheet. It is worth noting that when δ is equal to zero, the current study reverts to the no-slip condition. In this scenario, the velocity of the HFF matches the velocity at the surface of the sheet in accordance with the boundary condition (17), then $f'(0) = 1$. Interestingly, it is observed that the absence of slip conditions,

Table 4. Comparison of $-f''(0)$ for $\lambda = 1$.

Published paper	Olanrewaju [5]	Punith et al. [53]	Present study
$-f''(0)$	0.605848	0.6069352	0.6069

Table 5. Validation of δ against $-f''(0)$ when $S = 0$ and $S = 2$.

	$S = 0$			$S = 2$	
δ	Andersson [25]	Wang [26]	Present Study	Turkyilmazoglu [30]	Present Study
0.0	–	–	–	2.4142	2.4099
0.3	–	0.7010	0.7010	–	–
1.0	**–**	**0.4300**	**0.4305**	**0.6823**	**0.6816**
3.0	–	–	–	0.2870	0.2869
5.0	**0.1448**	**0.1450**	**0.1451**	**0.1822**	**0.1821**
50	0.0186	–	0.0187	–	–

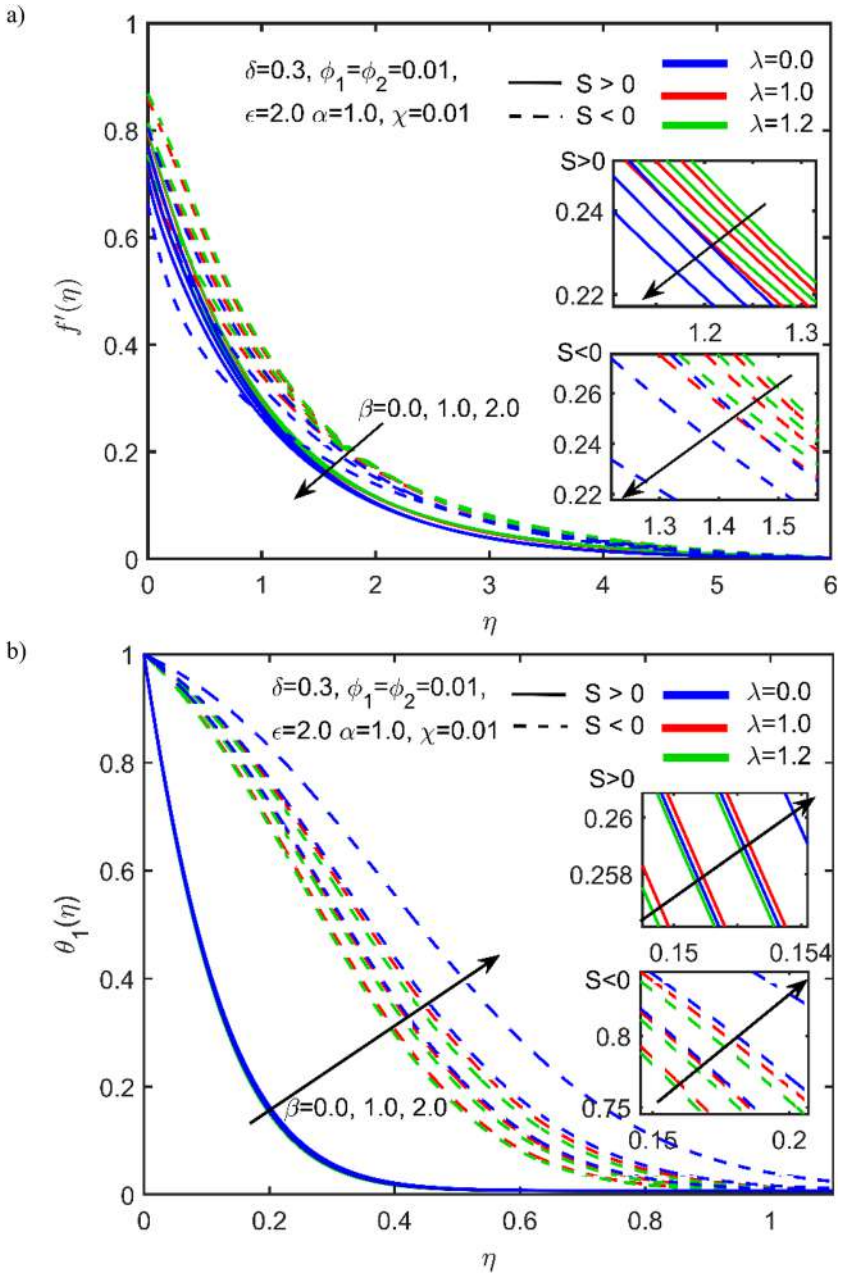

Figure 2. Velocity (a) and temperature (b) fields for parameter β.

when $\delta = 0$, leads to more incredible velocity compared to situations where $\delta > 0$. This trend aligns with the findings reported by Rajesh et al. [29]. Therefore, it is crucial to take into account partial velocity slip, particularly when managing the motion of the HFF in heat transfer processes. For example, this aspect can be employed to improve the elimination of cancer cells or tissues while minimizing harm to healthy tissue during cancer treatment. In addition, it is observed that the forced convection, when $\lambda = 0$ exhibits a faster decrease in $f'(\eta)$ as the parameter δ increases. The absence of buoyancy force causes nanoparticles in HFF to move to the surface of the sheet faster than in scenarios with natural convection and mixed convection, when $\lambda > 0$. The suction

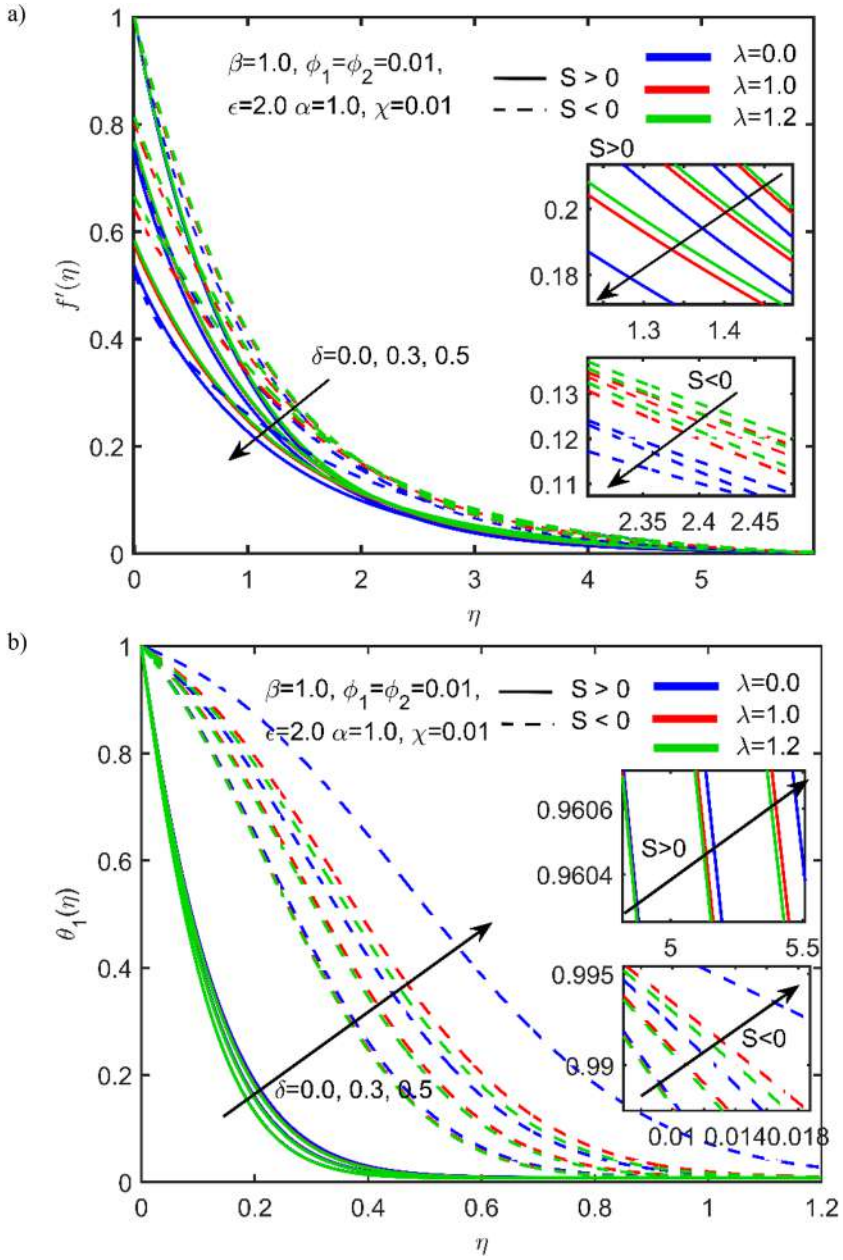

Figure 3. Velocity (a) and temperature (b) fields for parameter δ.

effect, when $S > 0$, leads to a quicker reduction in $f'(\eta)$ compared to when $S < 0$.

The pattern of $\theta_1(\eta)$ for the different values of the partial velocity slip parameter, δ is illustrated in Figure 3(b). The parameter δ modifies the characteristics of the HFF flow by releasing heat from the surface, consequently increasing the temperature within the HFF as the sheet stretches. Thereby, the thermal boundary layer elevates. This outcome is in good agreement with the numerical finding of hybrid nanofluid, as reported by Rajesh et al. [29]. It is evident that parameter δ enhances convective heat transfer between the HFF and the surrounding fluid. Therefore, the partial slip resulting from nanoparticle collisions with the surface becomes crucial in elevating the temperature of the HFF flow. Conversely, in the absence of slip conditions, when $\delta = 0$, the pattern of $\theta_1(\eta)$ is detected lower than when velocity slip is present, when $\delta > 0$. In the no-slip condition, the heat transfer primarily occurs through conduction, which is a slower heat transfer mechanism compared to convection. However, the convection fluid facilitated by slip conditions is more effective in carrying heat away from the surface, resulting in a higher $\theta_1(\eta)$ near the boundary. This phenomenon underlines the significance of surface roughness under the consideration of the parameter δ in intensifying fluid temperature. This is crucial in applications that maintain specific temperature ranges or gradients, such as in electronic cooling or biomedical treatments. Higher pattern of $\theta_1(\eta)$ is observed under forced convection conditions ($\lambda = 0$), as illustrated in Figure 3(b). This is attributed to forced convection, where fluid motion is externally induced, usually by stretching the sheet, resulting in the minimal influence of buoyancy force. This forced

flow enhances the heat transfer rate, resulting in a more pronounced temperature increase compared to natural or free convection and mixed convection, where fluid motion is driven by buoyancy forces with $\lambda > 0$. The injection process, when $S < 0$, contributes to higher values of $\theta_1(\eta)$ compared to the suction process, when $S > 0$. This is because the injection process drags in additional heat content to the HFF system, thereby increasing the thermal boundary layer.

4.4. Nanoparticles volume fraction (ϕ_2)

Figure 4(a) is plotted to analyze the influence of the nanoparticle volume fraction of the parameter ϕ_2 on $f'(\eta)$. It is ascertained that adding $CoFe_2O_4$ nanoparticles from 0% to 2% into the Fe_3O_4 ($\phi_1 = 1\%$) solution results in the reduction of $f'(\eta)$. The reason behind this is that the HFF becomes more viscous due to the incremental addition of $CoFe_2O_4$ nanoparticles, leading to additional aggregation and clustering in the HFF. Furthermore, the aggregated particles create obstacles in the fluid, hindering their ability to move freely. The increased nanoparticle concentration also disrupts momentum transfer within the HFF, particularly near the boundary layer. This disruption reduces the momentum boundary layer as the HFF encounters increased resistance. It is also detected that the HFF negatively affects the velocity of nanoparticles compared to ferrofluid, when $\phi_2 = 0$, primarily due to the faster reduction on $f'(\eta)$. This phenomenon can be attributed to the heightened presence of nanoparticles within the fluid, resulting in an overall increase in fluid viscosity. This finding aligns with the research conducted by Zainodin et al. [71] with a similar HFF flow. Furthermore, in Figure 4(a), it is illustrated that the momentum boundary layer is thinner in forced convection ($\lambda = 0$), followed by mixed convection ($\lambda = 1.0$) and natural convection ($\lambda = 1.2$). This phenomenon is attributed to the faster reduction of $f'(\eta)$ in cases without buoyancy forces. Moreover, the analysis reveals that the suction process ($S > 0$) results in a quicker diminishment of $f'(\eta)$ compared to the injection process ($S < 0$). This discrepancy arises from the removal of reactants inducing a reduction in viscosity within the HFF system, thereby causing the momentum boundary layer to move towards the sheet.

As depicted in Figure 4(b), changes in nanoparticle volume fraction within the fluid notably influence $\theta_1(\eta)$. Physically, increasing the nanoparticle volume fraction significantly enhances the overall thermal conductivity of the fluid, playing a vital role in improving heat transmission efficiency. As the parameter ϕ_2 rises, the convective heat transfer coefficient improves, contributing to an elevated $\theta_1(\eta)$ until the fluid reaches the temperature of the magnetic nanoparticle, T_c. Moreover, a higher nanoparticle volume fraction augments the contact points between nanoparticles, intensifying thermal interactions during fluid flow. This leads to the thickening of the thermal boundary layer as more heat transfers from the solid surface to the HFF system. It is also observed that $\theta_1(\eta)$ increases in the HFF when the volume of $CoFe_2O_4$ is introduced into the solution of Fe_3O_4 compared to the ferrofluid of Fe_3O_4 alone. The inclusion of $CoFe_2O_4$ nanoparticles in the Fe_3O_4 solution enhances the absorption and retention of heat effectively. This heightened capacity for heat absorption leads to a greater $\theta_1(\eta)$ as more thermal energy is retained within the HFF. It is observed that $\theta_1(\eta)$ is higher in forced convection, when $\lambda = 0$, compared to the case where $\lambda > 0$ for natural and mixed convection. Notably, the presence of an external force in the absence of buoyancy forces contributes to an increase in the thermal conductivity of the HFF, consequently leading to a thicker thermal boundary layer. The expansion of the temperature field is also observed during the injection process, when $S < 0$ than the suction process, when $S > 0$.

4.5. Local skin friction ($f''(0)$) and nusselt number ($\theta_1'(0) + \xi^2\theta_2'(0)$)

Table 6 presents the comparisons of local skin friction ($f''(0)$) and Nusselt number ($\theta_1'(0) + \xi^2\theta_2'(0)$) for different values of the parameter β, considering various S and λ in the respective cases. It should be noted that the presence of the FHD effect, when $\beta > 0$, increases the dimensionless quantity of local skin friction compared to the absence of the FHD effect, when $\beta = 0$. The introduction of the magnetic dipole alters the behavior of the fluid through magnetic forces, intensifying the movement of fluid particles near the surface. This heightened movement leads to increased frictional forces in HFF particles near the surface. Consequently, this increased shearing effect enhances momentum transfer, resulting in heightened skin friction. The study reveals that the enhancement of $f''(0)$ in forced convection ($\lambda = 0$) was 25.96%, followed by 28.06% in mixed convection ($\lambda = 1$) and 28.53% in natural convection ($\lambda = 1.2$) during the suction process at $S > 0$. Meanwhile, in the injection process at $S < 0$, it was observed that the enhancement of $f''(0)$ is higher than in the case of $S > 0$. The upsurge of β from 0 to 2 in the injection process enhances $f''(0)$ by 71.89% for $\lambda = 0$, 83% for $\lambda = 1$, and 87.08% for $\lambda = 1.2$.

Table 6 also illustrates that as $\beta > 0$ along with suction and injection conditions, results in a faster decrementation in $\theta_1'(0) + \xi^2\theta_2'(0)$ compared to $\beta = 0$ for various values of the parameter λ. This outcome signifies a reduction in the heat transfer rate. The interaction between the magnetic dipole and HFF introduces heightened forces, including magnetic and shear stress within the system. These intensified forces hinder the effective transfer of heat energy from the surface, thereby disrupting the convective heat transfer process.

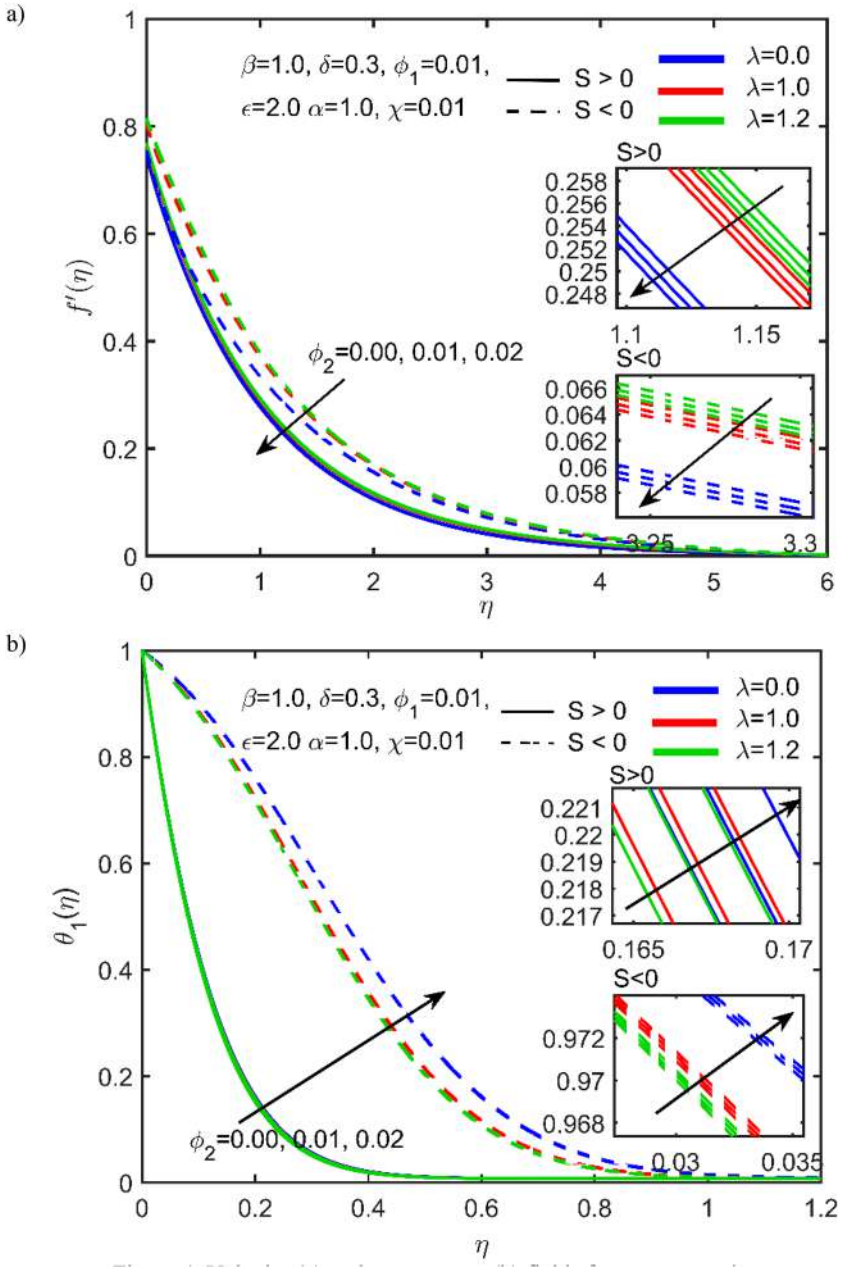

Figure 4. Velocity (a) and temperature (b) fields for parameter ϕ_2.

Table 6. Comparing the values of $-f''(0)$ and $-[\theta_1'(0)+\xi^2\theta_2'(0)]$ for various S and λ with respect to the parameter β.

		$\lambda = 0.0$		$\lambda = 1.0$		$\lambda = 1.2$	
β	Cases	$-f''(0)$	$-[\theta_1'(0)+\xi^2\theta_2'(0)]$	$-f''(0)$	$-[\theta_1'(0)+\xi^2\theta_2'(0)]$	$-f''(0)$	$-[\theta_1'(0)+\xi^2\theta_2'(0)]$
0.0	$S > 0$	0.7665	7.3537	0.6917	7.4448	0.6771	7.4633
	$S < 0$	0.6523	0.8950	0.4711	1.0232	0.4380	1.0460
1.0	$S > 0$	0.8645	7.1568	0.7876	7.2510	0.7725	7.2701
	$S < 0$	0.8669	0.7105	0.6575	0.8607	0.6205	0.8862
2.0	$S > 0$	0.9655	6.9597	0.8858	7.0610	0.8703	7.0809
	$S < 0$	1.1218	0.4980	0.8621	0.6903	0.8194	0.8351

It is noteworthy that the decrement in $\theta_1'(0)+\xi^2\theta_2'(0)$ is more pronounced under the influence of $S < 0$ than $S > 0$. This is attributed to the faster removal of the reactant from the HFF system, leading to a cut-off in the convective heat transfer rate. Additionally, it is observed that the presence of buoyancy force ($\lambda > 0$) inhibits the deterioration in $\theta_1'(0)+\xi^2\theta_2'(0)$ in contrast to the absence of buoyancy force ($\lambda = 0$) in both cases. The smallest reduction in $\theta_1'(0)+\xi^2\theta_2'(0)$ is noted when the buoyancy force is at its maximum in natural convection, occurring at $\lambda = 1.2$. This results in reductions of 5.12% and 20.16% for $S > 0$ and $S < 0$, respectively. In the case of mixed convection with $\lambda = 1.2$, the $\theta_1'(0)+\xi^2\theta_2'(0)$ decreases by 5.15% for $S > 0$ and 32.54% for $S < 0$. In forced convection without buoyancy force as $\lambda = 0$, the injection process leads to a higher decay in

$\theta_1'(0) + \xi^2\theta_2'(0)$ compared to the suction process. The decrement is observed to be 44.36% and 5.36% for $S < 0$ and $S > 0$, respectively.

5. Conclusion

The present investigation focuses on exploring the characteristics of a hybrid ferrofluid (HFF), specifically $Fe_3O_4 - CoFe_2O_4$, when introduced into a mixture of ethylene glycol (EG) and water. The research investigates the combined impact of a magnetic dipole effect and mixed convection. The presence of nanoscale particles induces slippage at the solid surface, and the use of suction and injection is crucial for stabilizing the HFF system. A mathematical formulation has been devised to depict the flow of the HFF over a stretching sheet, aiming to model the cooling and heating processes. Initially, the governing equations have been simplified into a set of nonlinear ordinary differential equations. These resulting equations are then numerically solved using the Keller box method. The study delves into the effects of ferrohydrodynamics, slip velocity, and the volume fraction of nanoparticles concerning mixed convection, suction, and injection effects. The investigation provides a thorough analysis and discussion of these parameters, yielding noteworthy findings such as

i. the presence of the ferrohydrodynamics (FHD) interaction, partial velocity slip, and nanoparticles volume fraction parameters significantly influences both the profiles of velocity and thermal in the HFF system,
ii. the velocity field diminishes with an increase in the parameters of FHD, partial velocity slip, and nanoparticles volume fraction, but an opposite trend is observed in the temperature profile,
iii. in forced convection, the momentum boundary layer becomes thinner as $\lambda = 0$, followed by mixed convection at $\lambda = 1$ and natural convection at $\lambda = 1.2$ across the investigated parameters of FHD, partial velocity slip, and nanoparticles volume fraction,
iv. the absence of the buoyancy force at $\lambda = 0$, consistently enhances the thermal boundary layer, contrasting with the maximum buoyancy force from $\lambda = 1$ to $\lambda = 1.2$ in different values of the parameters of FHD, partial velocity slip, and nanoparticles volume fraction,
v. the removal of reactants during the injection process as $S < 0$ results in an escalation of movement and heat content in the HFF system for the parameters of FHD, partial velocity slip, and nanoparticles volume fraction,
vi. the shear stress in the HFF system is directly correlated with the presence of the magnetic dipole within the FHD parameter, which ranges from 0 to 2, encompassing both suction and injection processes,
vii. convective heat transfer decreases with an increasing impact of FHD in both suction and injection cases,
viii. during the suction process, the local skin friction increases by 25.96%, 28.06%, and 28.53% for $\lambda = 0$, $\lambda = 1.0$ and $\lambda = 1.2$, respectively,
ix. forced convection, when $\lambda = 0$ exhibits a higher reduction in the Nusselt number by 44.36% during the suction process, when $S > 0$ compared to the injection process, when $S < 0$, which shows a reduction of 5.36%,
x. higher shear stress is detected during the injection process, when $S < 0$, particularly at the peak buoyancy force of natural convection.
xi. In the realm of medical treatment, incorporating parameters like FHD, partial velocity slip, and nanoparticles volume fraction improves the temperature distribution, allowing for regulated heat retention between 40 $\circ$ C to 45 $\circ$ C [49].
xii. With improved heat distribution, forced convection can reduce the time needed for hyperthermia treatment sessions. This not only enhances patient comfort but can also lead to more efficient treatment outcomes.
xiii. Utilizing suction intensity can reduce harm to healthy cells by limiting the movement of the HFF during cancer treatment after the removal of reactants from the body.

Overall, the study and understanding of the ferrohydrodynamic effect, mixed convection, and partial slip together with the suction and injection effect in magnetized hybrid ferrofluid must be taken into account. These parameters are crucial for optimizing the performance, efficiency, and reliability of various engineering systems and processes across a wide range of applications, particularly from electronics heating and cooling systems to solar thermal systems and environmental flows. For future studies, it is advisable to investigate the impact of supplementary variables under slip conditions, such as second-order velocity or nonlinear slip conditions, as suggested by Karniadakis et al. [84] and ternary nanofluids [85], as well as non-Newtonian fluids like Casson [16,86].

Acknowledgement

This research was funded by a grant from Universiti Teknologi Malaysia through vote number numbers Q.J130000.3854.31 J28 (UTMER).

Disclosure statement

No potential conflict of interest was reported by the author(s).

Funding

This work was supported by Universiti Teknologi Malaysia: [Grant Number].

Ethical approval

Given the theoretical nature of this study, it did not involve human or animal subjects. Consequently, no ethical approval was required.

Consent to participate not applicable

As this study is theoretical in nature, it did not involve direct participation from human or animal subjects.

Consent for publication not applicable

This theoretical study does not contain any individual person's data in any form (including any individual details, images, or videos).

References

[1] Janna WS. Engineering heat transfer. CRC Press; 2018. doi:10.1201/9781439883143
[2] Struchtrup H. Thermodynamics and energy conversion. Springer; 2014. doi:10.1007/978-3-662-43715-5
[3] Afridi MI, Qasim M, Khan I, et al. Entropy generation in magnetohydrodynamic mixed convection flow over an inclined stretching sheet. Entropy. 2017;19(1):1–11. doi:10.3390/e19010010
[4] Mahdy A. Unsteady mixed convection boundary layer flow and heat transfer of nanofluids due to stretching sheet. Nucl Eng Des. 2012;249:248–255. doi:10.1016/j.nucengdes.2012.03.025
[5] Olanrewaju P. Effects of internal heat generation on hydromagnetic non-darcy flow and heat transfer over a stretching sheet in the presence of thermal radiation and ohmic dissipation. World Appl Sci J. 2012;16:37–45.
[6] Daniel YS, Aziz ZA, Ismail Z, et al. Slip role for unsteady MHD mixed convection of nanofluid over stretching sheet with thermal radiation and electric field. Indian J Phys. 2020 ;94(2):195–207. doi:10.1007/s12648-019-01474-y
[7] Ishak A, Nazar R, Pop I. Unsteady mixed convection boundary layer flow due to a stretching vertical surface. Arab J Sci Eng. 2006;31(2):165–182.
[8] Chaudhary S, Choudhary MK. Partial slip and thermal radiation effects on hydromagnetic flow over an exponentially stretching surface with suction or blowing. Therm Sci. 2018;22(2):797–808. doi:10.2298/TSCI160127150C
[9] Gupta P, Gupta A. Heat and mass transfer on a stretching sheet with suction or blowing. Can J Chem Eng. 1977;55(6):744–746. doi:10.1002/cjce.5450550619
[10] Crane LJ. Flow past a stretching plate. Zeitschrift für Angewandte Mathematik und Physik ZAMP. 1970;21:645–647. doi:10.1007/BF01587695
[11] Elazem NYA. New exact and numerical solutions for the effect of suction or injection on flow of nanofluids past a stretching sheet. Nonlinear Eng. 2019;8(1):172–178. doi:10.1515/nleng-2017-0059
[12] Ibrahim W, Shankar B. MHD boundary layer flow and heat transfer of a nanofluid past a permeable stretching sheet with velocity, thermal and solutal slip boundary conditions. Comput Fluids. 2013;75:1–10. doi:10.1016/j.compfluid.2013.01.014
[13] Jha BK, Azeez LA, Oni MO. Unsteady hydromagnetic-free convection flow with suction/injection. J Taibah Univ Sci. 2019;13(1):136–145. doi:10.1080/16583655.2018.1545624
[14] Naramgari S, Sulochana C. MHD flow over a permeable stretching/shrinking sheet of a nanofluid with suction/injection. Alexandria Eng J. 2016;55(2):819–827. doi:10.1016/j.aej.2016.02.001
[15] Obalalu AM, Wahaab FA, Adebayo LL. Heat transfer in an unsteady vertical porous channel with injection/suction in the presence of heat generation. J Taibah Univ Sci. 2020;14(1):541–548. doi:10.1080/16583655.2020.1748844
[16] Kamis NI, Rawi NA, Jiann LY, et al. Thermal characteristics of an unsteady hybrid nano-casson fluid passing through a stretching thin-film with mass transition. Adv Res Fluid Mech Therm Sci. 2023;104(2):36–50. doi:10.37934/arfmts.104.2.3650
[17] Guled C, Tawade J, Kumam P, et al. The heat transfer effects of MHD slip flow with suction and injection and radiation over a shrinking sheet by optimal homotopy analysis method. Results Eng. 2023;18:101173–101183. doi:10.1016/j.rineng.2023.101173
[18] Maranna T, Mahabaleshwar US, Ravichandra Nayakar SN, et al. An influence of radiation and magnetohydrodynamic flow of hybrid nanofluid past a stretching/shrinking sheet with mass transpiration. J Appl Math Mech. 2023;103(12):e202300140–e202300140. doi:10.1002/zamm.202300140
[19] Maranna T, Sneha K, Mahabaleshwar U, et al. An impact of heat and mass transpiration on magnetohydrodynamic viscoelastic fluid past a permeable stretching/shrinking sheet. Heat Transfer. 2023;52(3):2231–2248. doi:10.1002/htj.22782
[20] Kamis NI, Basir MFM, Shafie S, et al. Suction effect on an unsteady casson hybrid nanofluid film past a stretching sheet with heat transfer analysis. IOP Conf Ser: Mater Sci Eng. 2021;1078(1):012019–012029. IOP Publishing.
[21] Siddiqui AA, Turkyilmazoglu M. Slit flow and thermal analysis of micropolar fluids in a symmetric channel with dynamic and permeable. Int Commun Heat Mass Transfer. 2022;132:105844–105857. doi:10.1016/j.icheatmasstransfer.2021.105844
[22] Madhu M, Kishan N, Chamkha AJ. Unsteady flow of a Maxwell nanofluid over a stretching surface in the presence of magnetohydrodynamic and thermal radiation effects. Propuls Power Res. 2017;6(1):31–40. doi:10.1016/j.jppr.2017.01.002
[23] Zhang W-M, Meng G, Wei X. A review on slip models for gas microflows. Microfluid Nanofluid. 2012;13:845–882. doi:10.1007/s10404-012-1012-9
[24] Navier C. Mémoire sur les lois du mouvement des fluides. éditeur inconnu; 1822.
[25] Andersson HI. Slip flow past a stretching surface. Acta Mech. 2002;158(1-2):121–125. doi:10.1007/BF01463174
[26] Wang C. Flow due to a stretching boundary with partial slip—an exact solution of the navier–stokes equations. Chem Eng Sci. 2002;57(17):3745–3747. doi:10.1016/S0009-2509(02)00267-1
[27] Thompson PA. Troian SM. A general boundary condition for liquid flow at solid surfaces. Nature. 1997;389(6649):360–362. doi:10.1038/38686
[28] Yazdi M, Abdullah S, Hashim I, et al. Slip MHD liquid flow and heat transfer over nonlinear permeable stretching

surface with chemical reaction. Int J Heat Mass Transfer. 2011;54(15-16):3214–3225. doi:10.1016/j.ijheatmasstransfer.2011.04.009
[29] Sharma R, Ishak A, Pop I. Partial slip flow and heat transfer over a stretching sheet in a nanofluid. Math Probl Eng. 2013;2013:724547–724555. doi:10.1155/2013/724547
[30] Turkyilmazoglu M. Heat and mass transfer of MHD second order slip flow. Comput Fluids. 2013;71:426–434. doi:10.1016/j.compfluid.2012.11.011
[31] Zeeshan A, Majeed A, Ellahi R, et al. Mixed convection flow and heat transfer in ferromagnetic fluid over a stretching sheet with partial slip effects. Therm Sci. 2018;22–26(Part A):2515–2526. doi:10.2298/TSCI160610268Z
[32] Malkin AY, Patlazhan SA. Wall slip for complex liquids – phenomenon and its causes. Adv Colloid Interface Sci. 2018;257:42–57. doi:10.1016/j.cis.2018.05.008
[33] Choi SU, Eastman JA. Enhancing thermal conductivity of fluids with nanoparticles. Argonne National Lab.(ANL), Argonne, IL (United States); 1995.
[34] Mahian O, Kolsi L, Amani M, et al. Recent advances in modeling and simulation of nanofluid flows-part I: fundamentals and theory. Phys Rep. 2019;790:1–48. doi:10.1016/j.physrep.2018.11.004
[35] Maxwell JC. A treatise on electricity and magnetism. Vol. 1. Clarendon Press; 1873.
[36] Suneetha S, Subbarayudu K, Bala Anki Reddy P. Hybrid nanofluids development and benefits: A comprehensive review. J Therm Eng. 2022;8(3):445–455. doi:10.18186/thermal.1117455
[37] Ali HM. Hybrid nanofluids for convection heat transfer. Academic Press; 2020.
[38] Sarkar J, Ghosh P, Adil A. A review on hybrid nanofluids: recent research, development and applications. Renewable Sustainable Energy Rev. 2015;43:164–177. doi:10.1016/j.rser.2014.11.023
[39] Philip J, Shima P, Raj B. Enhancement of thermal conductivity in magnetite based nanofluid due to chainlike structures. Appl Phys Lett. 2007;91(20):203108–203112. doi:10.1063/1.2812699
[40] Philip J. Magnetic nanofluids: recent advances, applications, challenges, and future directions. Adv Colloid Interface Sci. 2022:102810–102854. doi:10.1016/j.cis.2022.102810
[41] Gui NGJ, Stanley C, Nguyen N-T, et al. Ferrofluids for heat transfer enhancement under an external magnetic field. Int J Heat Mass Transfer. 2018;123:110–121. doi:10.1016/j.ijheatmasstransfer.2018.02.100
[42] Raj K, Boulton R. Ferrofluids – properties and applications. Mater Des. 1987;8(4):233–236. doi:10.1016/0261-3069(87)90139-7
[43] Alsoy-Akgün N. Effect of an uniform magnetic field on unsteady natural convection of nanofluid. J Taibah Univ Sci. 2019;13(1):1073–1086. doi:10.1080/16583655.2019.1682342
[44] Kabeel AE, El-Said EMS, Dafea SA. A review of magnetic field effects on flow and heat transfer in liquids: present status and future potential for studies and applications. Renewable Sustainable Energy Rev. 2015;45:830–837. doi:10.1016/j.rser.2015.02.029
[45] Rosensweig R. Ferrohydrodynamics Cambridge Univ. Press, Cambridge. 1985:344.
[46] Iftikhar B, Siddiqui MA, Javed T. Dynamics of magnetohydrodynamic and ferrohydrodynamic natural convection flow of ferrofluid inside an enclosure under non-uniform magnetic field. Alexandria Eng J. 2023;66:523–536. doi:10.1016/j.aej.2022.11.011
[47] Chao D, Zhu C, Yang P, et al. Array of nanosheets render ultrafast and high-capacity Na-ion storage by tunable pseudocapacitance. Nat Commun. 2016;7(1):12122–12130. doi:10.1038/ncomms12122
[48] Raj K, Moskowitz B, Casciari R. Advances in ferrofluid technology. J Magn Magn Mater. 1995;149(1-2):174–180. doi:10.1016/0304-8853(95)00365-7
[49] Moradiya M, Ladani A, Ladani J, et al. New way to treat cancer: magnetic nanoparticle based hyperthermia. J Chem Sci Eng. 2019;2(1):58. À60.
[50] Vijayan PP, Radhamany AS, Beeran AE, et al. Magnetic nanoparticles-based coatings. In: Nanotechnology in the automotive industry. Elsevier; 2022. p. 317–343. doi:10.1016/B978-0-323-90524-4.00016-5
[51] Zhou K, Zhou X, Liu J, et al. Application of magnetic nanoparticles in petroleum industry: a review. J Pet Sci Eng. 2020;188:106943–106970. doi:10.1016/j.petrol.2020.106943
[52] Neuringer JL, Rosensweig RE. Ferrohydrodynamics. Phys Fluids. 1964;7(12):1927–1937. doi:10.1063/1.1711103
[53] Gowda RP, Kumar RN, Prasannakumara B, et al. Exploring magnetic dipole contribution on ferromagnetic nanofluid flow over a stretching sheet: An application of stefan blowing. J Mol Liq. 2021;335:116215–116223. doi:10.1016/j.molliq.2021.116215
[54] Andersson H, Valnes O. Flow of a heated ferrofluid over a stretching sheet in the presence of a magnetic dipole. Acta Mech. 1998;128(1-2):39–47. doi:10.1007/BF01463158
[55] Seleznyova K, Strugatsky M, Kliava J. Modelling the magnetic dipole. Eur J Phys. 2016;37(2):025203–025218. doi:10.1088/0143-0807/37/2/025203
[56] Davidson PA. Introduction to magnetohydrodynamics. Vol. 55. Cambridge University Press; 2016.
[57] Muhammad N, Nadeem S, Mustafa M. Analysis of ferrite nanoparticles in the flow of ferromagnetic nanofluid. PLoS One. 2018;13(1):e0188460–e0188483. doi:10.1371/journal.pone.0188460
[58] Padervand M, Vossoughi M, Yousefi H, et al. An experimental and theoretical study on the structure and photoactivity of XFe 2 O 4 (X = Mn, Fe, Ni. Co, and Zn) structures. Russ J Phys Chem A. 2014;88:2451–2461. doi:10.1134/S0036024414130184
[59] Dinarvand M, Abolhasani M, Hormozi F, et al. Experimental investigation and performance comparison of Fe3O4/water and CoFe2O4/water ferrofluids in presence of a magnetic field in a cooling system. J Taiwan Inst Chem Eng. 2023: 104927–104936. doi:10.1016/j.jtice.2023.104927
[60] Amiri S, Shokrollahi H. The role of cobalt ferrite magnetic nanoparticles in medical science. Mater Sci Eng C. 2013;33(1):1–8. doi:10.1016/j.msec.2012.09.003
[61] Kumar K A, Sandeep N, Sugunamma V, et al. Effect of irregular heat source/sink on the radiative thin film flow of MHD hybrid ferrofluid. J Therm Anal Calorim. 2020;139:2145–2153. doi:10.1007/s10973-019-08628-4
[62] Anwar T, Kumam P, Thounthong P. Fractional modeling and exact solutions to analyze thermal performance of Fe3O4-MoS2-water hybrid nanofluid flow over an inclined surface with ramped heating and ramped boundary motion. IEEE Access. 2021;9:12389–12404. doi:10.1109/ACCESS.2021.3051740
[63] Tahir H, Khan U, Din A, et al. Hybridized two phase ferromagnetic nanofluid with NiZnFe2O4 and MnZnFe2O4. Ain Shams Eng J. 2021;12(3):3063–3070. doi:10.1016/j.asej.2020.10.026

[64] Khan M I, Qayyum S, Shah F, et al. Marangoni convective flow of hybrid nanofluid (MnZnFe2O4-NiZnFe2O4-H2O) with darcy forchheimer medium. Ain Shams Eng J. 2021;12(4):3931–3938. doi:10.1016/j.asej.2021.01.028

[65] Yang J, Abdelmalek Z, Muhammad N, et al. Hydrodynamics and ferrite nanoparticles in hybrid nanofluid. Int Commun Heat Mass Transfer. 2020;118:104927–104936. doi:10.1016/j.icheatmasstransfer.2020.104883

[66] Zainodin S, Jamaludin A, Nazar R, et al. Impact of heat source on mixed convection hybrid ferrofluid flow across a shrinking inclined plate subject to convective boundary conditions. Alexandria Eng J. 2024;87:662–681. doi:10.1016/j.aej.2023.12.057

[67] Mansourian M, Dinarvand S, Pop I. Aqua cobalt ferrite/Mn–Zn ferrite hybrid nanofluid flow over a nonlinearly stretching permeable sheet in a porous medium. J Nanofluids. 2022;11(3):383–391. doi:10.1166/jon.2022.1841

[68] Zhao T-H, Khan MI, Qayyum S, et al. Comparative study of ferromagnetic hybrid (manganese zinc ferrite, nickle zinc ferrite) nanofluids with velocity slip and convective conditions. Phys Scr. 2021;96(7):075203–075217. doi:10.1088/1402-4896/abf26b

[69] Kumar TS. Hybrid nanofluid slip flow and heat transfer over a stretching surface. Partial Differ Equ Appl Math. 2021;4:100070–100078. doi:10.1016/j.padiff.2021.100070

[70] Ezhil K, Thavada SK, Ramakrishna SB. MHD slip flow and heat transfer of Cu-Fe3O4/ethylene glycol-based hybrid nanofluid over a stretching surface. Biointerface Res Appl Chem. 2021;11(4):11956–11968. doi:10.33263/BRIAC114.1195611968

[71] Zainodin S, Jamaludin A, Nazar R, et al. Effects of higher order chemical reaction and slip conditions on mixed convection hybrid ferrofluid flow in a darcy porous medium. Alexandria Eng J. 2023;68:111–126. doi:10.1016/j.aej.2023.01.011

[72] Manzoor U, Imran M, Muhammad T, et al. Heat transfer improvement in hybrid nanofluid flow over a moving sheet with magnetic dipole. Waves Random Complex Media. 2021: 1–15. doi:10.1080/17455030.2021.1991602

[73] Cebeci T, Bradshaw P. Physical and computational aspects of convective heat transfer. New York: Springer; 1988. (ed. s, editor.). doi:10.1007/978-1-4612-3918-5

[74] Shoghl S N, Jamali J, Keshavarz Moraveji M. Electrical conductivity, viscosity, and density of different nanofluids: An experimental study. Exp Therm Fluid Sci. 2016;74:339–346. doi:10.1016/j.expthermflusci.2016.01.004

[75] Çolak AB, Yildiz O, Bayrak M, et al. Experimental study on the specific heat capacity measurement of water-based al2o3-cu hybrid nanofluid by using differential thermal analysis method. Curr Nanosci. 2020;16(6):912–928. doi:10.2174/1573413715666191118105331

[76] Colak AB. Experimental study for thermal conductivity of water-based zirconium oxide nanofluid: developing optimal artificial neural network and proposing new correlation. Int J Energy Res. 2021;45(2):2912–2930. doi:10.1002/er.5988

[77] Tiwari RK, Das MK. Heat transfer augmentation in a two-sided lid-driven differentially heated square cavity utilizing nanofluids. Int J Heat Mass Transfer. 2007;50(9-10):2002–2018. doi:10.1016/j.ijheatmasstransfer.2006.09.034

[78] Brinkman HC. The viscosity of concentrated suspensions and solutions. J Chem Phys. 1952;20(4):571–571. doi:10.1063/1.1700493

[79] Maxwell JC. Electricity and magnetism. Vol. 2. Dover New York; 1954.

[80] Neuringer JL. Some viscous flows of a saturated ferrofluid under the combined influence of thermal and magnetic field gradients. Int J Nonlinear Mech. 1966;1(2):123–137. doi:10.1016/0020-7462(66)90025-4

[81] Chen T, Mucoglu A. Analysis of mixed forced and free convection about a sphere. Int J Heat Mass Transfer. 1977;20(8):867–875. doi:10.1016/0017-9310(77)90116-8

[82] Kamis NI, Jiann LY, Shafie S, et al. Numerical simulation of convection hybrid ferrofluid with magnetic dipole effect on an inclined stretching sheet. Alexandria Eng J. 2023;76:19–33. doi:10.1016/j.aej.2023.06.030

[83] Kamis NI, Jiann LY, Shafie S, et al. Comparative analysis of Fe3O4/CoFe2O4 and NiZnFe2O4/MnZnFe2O4 hybrid ferro-nanofluids flow under magnetic dipole effect over a slip stretching sheet. Case Stud Therm Eng. 2023;51:103580–103596. doi:10.1016/j.csite.2023.103580

[84] Karniadakis G, Beskok A, Aluru N. Microflows and nanoflows: fundamentals and simulation. Vol. 29. Springer Science & Business Media; 2006.

[85] Manjunatha S, Puneeth V, Gireesha B, et al. Theoretical study of convective heat transfer in ternary nanofluid flowing past a stretching sheet. J Appl Comput Mech. 2022;8(4):1279–1286.

[86] Idowu AS, Akolade MT, Abubakar JU, et al. MHD free convective heat and mass transfer flow of dissipative casson fluid with variable viscosity and thermal conductivity effects. J Taibah Univ Sci. 2020;14(1):851–862. doi:10.1080/16583655.2020.1781431